N. J. Hurd and P. E. Irving**

Micromechanisms and Fatigue Performance of a Quenched and Tempered Steel under Tension plus Torsion Loading

REFERENCE Hurd, N. J. and Irving, P. E., **Micromechanisms and fatigue performance of a quenched and tempered steel under tension plus torsion loading,** *Biaxial and Multiaxial Fatigue*, EGF 3 (Edited by M. W. Brown and K. J. Miller), 1989, Mechanical Engineering Publications, London, pp. 319–333.

ABSTRACT Multiaxial tension plus torsion fatigue tests have been performed on smooth specimens of a quenched and tempered steel with varying ratios of imposed shear strain to axial strain. The experimental results have been correlated using a parameter that is based on critical plane theories of multiaxial fatigue. A good correlation is achieved, but it does not reflect the micromechanisms of fatigue crack growth that occur.

Replica techniques have been employed to monitor the development of cracking for lives close to 10^5 cycles. It has been found that if the ratio of the imposed shear to axial strain is 0.5 or 1.5, the behaviour is as observed in uniaxial tests, but if this ratio is 4 the behaviour more closely resembles that observed in pure torsion. For this latter ratio, longer surface crack lengths are found at a given fraction of total life.

Potential interactive effects have been investigated by changing the imposed strain ratio during a test. It is found that some interaction does occur, but that shear cracks are not as damaging as their surface lengths suggest.

Introduction

Many automotive components experience multiaxial fatigue loadings in service and this represents a considerable incentive for the development of multiaxial fatigue life prediction methodologies. A convenient method of achieving this aim is to extend the concepts of the local strain-life approach to multiaxial situations. The strain-life approach has been used for fatigue life prediction with considerable success within the ground vehicle industry (**1**)–(**4**). Unfortunately, a validated approach is limited to cases where the loading at the critical location is approximately uniaxial (**3**) and, consequently, considerable efforts are being made to extend these and other concepts to multiaxial fatigue (**5**).

Much of this effort has been devoted to developing parameters that are able to correlate the multiaxial fatigue data. The cyclic shear strain range and the strain normal to the crack path have been identified as important parameters in multiaxial fatigue (**6**), and prediction methods are currently being developed based upon these concepts (**7**)–(**10**). Often, uniaxial fatigue data are employed as the material data in such predictions.

* GKN Technology Limited, Birmingham New Road, Wolverhampton WV4 6BW, UK.

The development of understanding of the micromechanisms that occur in multiaxial fatigue is as important as development of the parametric approach. Gaining insight into the mechanisms will allow boundaries to be set to the safe use of predictive schemes, and assist identification of areas where further work is required. This is particularly important in multiaxial fatigue, since the materials encountered are generally anisotropic, and multiaxial stressing can exacerbate the anisotropy of the material response. For example, the conventional choice of specimen orientation when testing wrought steels results in specimens with the inclusions aligned parallel to the longitudinal axis. Uniaxial fatigue crack growth then occurs perpendicular to the aligned inclusions, but torsional fatigue crack growth is generally found to occur along them (**11**). This is entirely appropriate to many components, where the inclusions at the critical location are found to be deliberately aligned in this manner.

Previous work has shown that the micromechanisms of fatigue failure of a medium strength (970 MPa ultimate tensile strength) low alloy forging steel to BS970 605H32, differ markedly between uniaxial and torsional loadings (**11**). Initiation and early growth in torsion were found to occur on shear planes, along the inclined inclusions. Growth was by Mode II along the specimen surface and by Mode III into the specimen in fracture mechanics terms. Subsequent crack growth generally remained on shear planes, and, in the terminology of Forsyth (**12**), a Stage I/Stage II transition was observed only at lives in excess of 10^5 cycles. This is in contrast to the predominantly Mode I, Stage II growth observed in uniaxial fatigue tests. In addition, surface crack lengths were found to be appreciably longer at a given fraction of life than for uniaxial loading. Cracks of 100 μm surface length were found to be present in torsion at approximately 10 per cent of total life, for lives in the range 10^4–10^5 cycles (**11**). Approximately 50 per cent of the total life was spent in growth of cracks in excess of 1 mm surface length, whereas in uniaxial tests 1 mm cracks occur relatively late in life. Similiar observations have recently been made on another engineering steel (**13**).

In this work multiaxial fatigue tests were performed on 605H32 steel so as to investigate micromechanisms under more general multiaxial loading. The development of fatigue cracking was also studied. Three strain ratios (λ) were employed, and crack development was monitored using replica techniques. The correlation of all the experimental multiaxial fatigue data was the first objective. The possibility of employing relatively simple parametric descriptions based on critical plane theories is currently being investigated in some detail. The Kandil *et al.* parameter (**14**) was employed, due to its success in correlating other material data (**7**)(**8**). This parameter is based on the proposal (**6**) that the range of maximum shear strain ($\Delta\gamma_m$) governs plastic deformation and, hence, fatigue crack nucleation and propagation, while the tensile strain (ε_n) normal to the plane of maximum shear encourages crack growth. The multiaxial fatigue performance then depends on these two variables. The simplest specific form for this dependence, as proposed by Socie *et al.* (**7**)(**8**), is

employed in the present work. This is because such a relatively simple form will be beneficial for a life prediction scheme which is intended to be ultimately employed for variable amplitude loadings.

The degree of correlation is discussed, and then assessed in the light of the observed micromechanisms at fatigue lives close to 10^5 cycles. The differing modes of growth that occur for the various strain ratios are compared. The difference in behaviour implies that interactions which reduce the overall life could occur if a service load history imposes differing strain ratios on a component. This was investigated by employing tests for which the strain ratio is changed during the test. Two test levels were chosen, which gave equivalent lives at strain ratios (λ) of 0.5 and 4. Tests were performed in which a set number of cycles at one ratio was followed by cycling to failure at the second. The results are discussed in terms of the observed micromechanisms and in the context of the life prediction.

Notation

γ_m	Maximum shear strain
ε_n	Normal strain across the plane of maximum shear
λ	Ratio of the applied shear strain amplitude to the axial strain amplitude
N	Applied cycles
N_f	Number of cycles to failure
$\Delta\sigma/2$	Applied tensile stress amplitude
$\Delta\tau/2$	Applied shear stress amplitude

Experimental procedure

The material employed in this work was BS970 605H32, a medium carbon, low-alloy, quenched and tempered steel typical of those employed in many automotive applications. The chemical composition (wt%) was 0.38 C, 0.21 Si, 1.62 Mn, 0.035 P, 0.045 S, 0.16 Ni, 0.15 Cr, 0.26 Mo, balance Fe. The steel was heat-treated by austenitising specimen blanks for one hour at 850°C, followed by oil quenching and tempering for two hours at 600°C. The resultant tensile properties achieved were an ultimate tensile strength of 972 MPa, a 0.2 per cent proof strength of 891 MPa, and 63 per cent reduction in area. A tempered martensitic microstructure was obtained by this heat treatment. The test specimens were machined out of rolled bar with the longitudinal axis of the specimen lying in the direction of working. Consequently, the fatigue test specimens had the inclusions aligned in the direction of the longitudinal axis. These inclusions included elongated manganese sulphides, and also strings of oxides. Final machining was performed after heat treatment to eliminate any potential problems associated with decarburisation of the specimen surface.

Uniaxial strain–life data and torsional shear strain–life for this material have been reported previously (**11**). A servohydraulic tension–torsion machine, of

200 kN axial load capacity and 2000 Nm torque capacity, was employed for the multiaxial fatigue testing. Strain-controlled fatigue tests were performed on 12.5 mm diameter parallel sided specimens. Failure was identified with separation of the specimen. The extensometer allowed both the shear strain and the direct strain applied to the specimen to be controlled independently, and tests were performed with the strains in-phase. In the high strain tests, an effective Poissons ratio was assumed for the calculation of principal strains (**7**).

Stress-controlled tests were performed for fatigue lives close to or greater than 10^5 cycles. These tests were performed on 10 mm diameter, parallel-sided, specimens, and they allowed easy replication of the specimen surface so that the development of the fatigue cracks could be monitored in detail. In this regime of life, it was found that the results of these stress-controlled tests agreed well with the strain-controlled tests.

Cellulose acetate replicas were employed to monitor fatigue crack development. The replicas were taken at regular intervals throughout each test, at intervals chosen to yield around 15 replicas per test. The replicas were examined under transmitted light, and the length of the microcracks measured using a calibrated graticule. The sites at which replicas indicated fatigue cracks had initiated were examined in the scanning electron microscope.

Results

Correlation of the fatigue data

The uniaxial strain–life data, and torsional shear strain–life data, have been combined with the multiaxial tension plus torsion fatigue test data in Fig. 1, to assess how well all the fatigue data were correlated by the Kandil *et al.* parameter (**14**). The general form of this parameter is

$$\left(\frac{\gamma_m}{2g}\right)^j + \left(\frac{\varepsilon_n}{h}\right)^j = 1 \tag{1}$$

where g, h, and j are material parameters which are fatigue life dependent. However, Socie *et al.* (**7**)(**8**) have employed a simple specific form of this equation with some success for SAE 1045 steel (**7**) and Inconel 718 (**8**). This specific form, which is adopted in this work, is that, at a given fatigue life, for in phase tests with no mean stress

$$\Delta(\gamma_m + \varepsilon_n) = \text{a constant} \tag{2}$$

By simply combining the maximum shear strain and the strain acting across the plane of maximum shear, the parameter emphasises the physical importance of these variables in multiaxial fatigue (**6**). This parameter was chosen rather than the parameter of similar form proposed by Lohr and Ellison (**15**) because, in this material, fatigue crack initiation and growth has been observed to occur on the maximum shear planes, rather than on the planes predicted by the Lohr–Ellison approach.

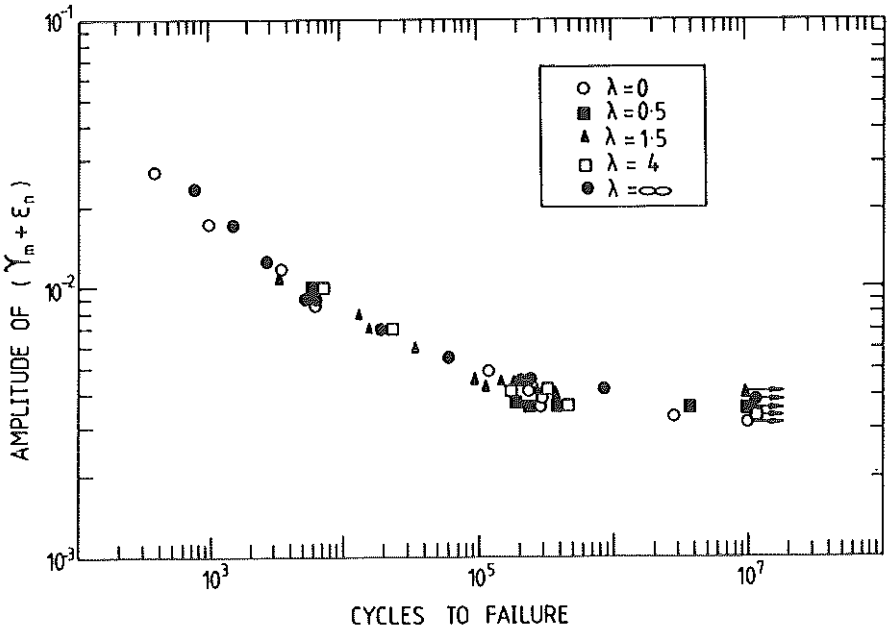

Fig 1 Plot of the amplitude of the Kandil *et al.* parameter ($\gamma_m + \varepsilon_n$) against fatigue life for all strain ratios employed in the test programme

The fatigue data ranges from failure lives of 500 cycles up to the fatigue limit. It can be seen that a satisfactory correlation has been achieved, in that the data are correlated within a factor of two on life at short and intermediate lives, up to 5×10^5 cycles. As the fatigue limit is approached, the scatter on life becomes considerably greater, and there is a scatter of approximately 26 per cent on the fatigue strength at 10^7 cycles. For such a steel, it is not unusual for the scatter on life to increase markedly as the fatigue limit is approached; scatter on life by factors of 10 to 1 between maximum and minimum observed life are quoted as being typical (**16**).

Micromechanisms

While the fatigue data were correlated relatively successfully, a general life prediction scheme needs to be related to the micromechanisms of fatigue crack initiation and growth that occur. The previous work showed that the behaviour of the material under uniaxial and torsional loading was quite different. To investigate the micromechanisms under multiaxial tension plus torsion loading, combinations of stresses were chosen to give lives close to 10^5 cycles. Tests were performed under stresses equivalent to three values of strain ratio, namely 0.5, 1.5, and 4, and replicas were used to monitor the growth of the cracks. It should

be noted that stress levels were chosen to yield equivalent lives in order that the following comparisons do not depend upon an assumed correlating parameter.

Tests at a strain ratio of 0.5

The crack size versus cycles data obtained from testing at a strain ratio of 0.5 is illustrated in Fig. 2. The behaviour is typical of that observed in uniaxial fatigue, with the surface crack length reaching 100 μm at 50 per cent of the life, and 1 mm close to failure (approximately 90 per cent of life). Fatigue crack initiation was observed to occur at inclusions, and the macroscopic mode of growth from the inclusions (Fig. 3(a)) was found to be perpendicular to the direction of the maximum principal stress; that is, by Mode I, in fracture

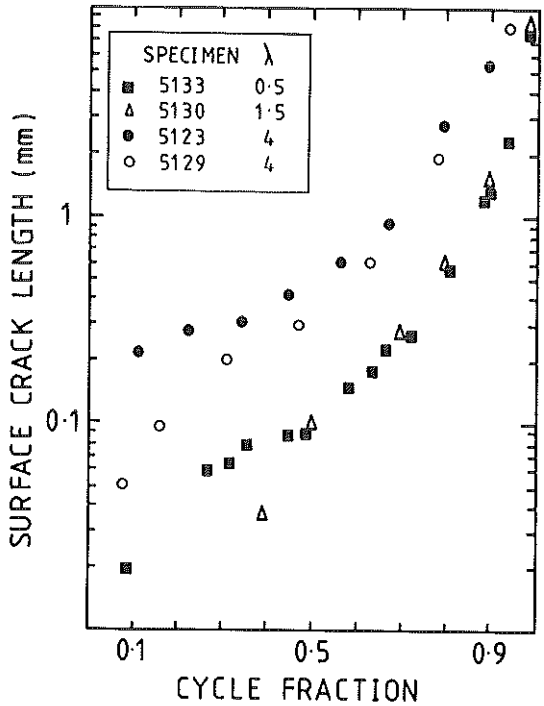

Fig 2 Plots of surface length versus cycle fraction obtained from the replica tests.

Specimen 5133: $\lambda = 0.5$, $\frac{\Delta\sigma}{2} = 433$ MPa, $\frac{\Delta\tau}{2} = 85$ MPa, $N_f = 221\,200$

Specimen 5130: $\lambda = 1.5$, $\frac{\Delta\sigma}{2} = 387$ MPa, $\frac{\Delta\tau}{2} = 228$ MPa, $N_f = 100\,200$

Specimen 5123: $\lambda = 4$, $\frac{\Delta\sigma}{2} = 201$ MPa, $\frac{\Delta\tau}{2} = 306$ MPa, $N_f = 89\,500$

Specimen 5129: $\lambda = 4$, $\frac{\Delta\sigma}{2} = 184$ MPa, $\frac{\Delta\tau}{2} = 288$ MPa, $N_f = 128\,000$

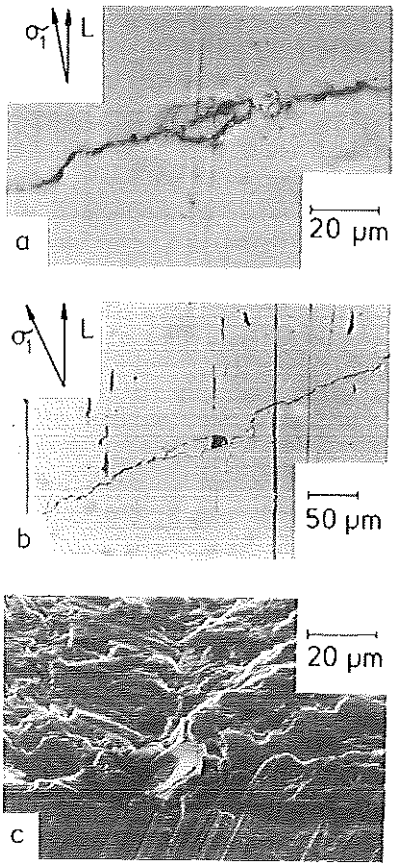

Fig 3 Fractographs: (a) replica taken from specimen 5133 at 198 000 cycles showing the inclusion that initiated the fatigue crack; (b) replica taken from specimen 5130 showing the inclusion that initiated fatigue cracking and the orientation of growth; (c) inclusion that initiated fatigue cracking in a test at $\lambda = 1.5$. The longitudinal axis is marked L on the replicas, and the direction of the principal axes is also marked

mechanics terminology. No evidence could be found for any marked Stage I growth from the inclusions. Examples of highly localised Stage I growth, over a few microns from initiating inclusions, have been reported in high strength steels (**17**). It is likely that rubbing of the fracture surfaces as the crack propagates would obscure any growth into the specimen over such a scale.

The inclusions that initiated fatigue cracking were found to be in the size range 20–50 μm, both for this strain ratio and the others. Energy-dispersive X-ray analysis was performed on representative fracture surfaces, to determine the nature of the inclusions. This showed that the inclusions were of the calcium aluminate type. Such inclusions are known to be among the most detrimental to the resistance to fatigue crack initiation (**16**)–(**19**) of high strength steels.

Tests at a strain ratio of 1.5

Crack size versus cycles data obtained by testing at a strain ratio of 1.5 is illustrated in Fig. 2. Again, the behaviour is similar to that obtained in uniaxial fatigue, with surface lengths of 100 μm and 1 mm being reached at 50 per cent and 85 per cent of the cycles to failure, respectively. Fatigue crack initiation occurred at inclusions of the calcium aluminate type. Fatigue crack growth very close to the inclusions was relatively complicated in orientation, typical examples begin shown in Figs 3(b) and 3(c). The macroscopic growth quickly became oriented normal to the maximum principal stress. Testing at this strain ratio showed a tendency towards multiple cracking, with cracks reaching similar sizes close to separation of the specimen.

Tests at a strain ratio of 4

Crack size versus cycles to failure data obtained at a strain ratio of 4 are illustrated in Fig. 2. The surface crack length development is now quite different. Cracks of 100 μm surface length are developed by 10–20 per cent of life, while millimetre-sized cracks develop by 70 per cent of life. These fractions of life are typical of those observed previously in this material under pure torsional loadings (**11**).

The plane of initial growth also differs from the previous two strain states. Initiation was again found to occur at oxide inclusions, but initial growth now occurs in the longitudinal shear plane, Fig. 4. Often this apparently occurred by the linking of the oxide inclusions aligned in this direction. After limited growth in this orientation, for typically 115–220 μm, the crack orientation switched to growth normal to the maximum principal stress. This occurred relatively early in life, so that 69–78 per cent of the life was spent in propagation normal to the maximum principal stress. Again, there was a tendency towards multiple cracking.

Tests at varying strain ratios

The difference in the development of the fatigue cracks for the different strain ratios implies that tests in which the strain ratio is varied could result in shorter lives than would be expected from a simple summation of fatigue damage. This is because, for the strain ratio of 4, premature initiation occurs compared to the other ratios. This could render the use of a correlating parameter, such as that employed in Fig. 1, non-conservative. This was investigated by performing tests in which the strain ratio was varied.

Initial cycles were applied at one strain ratio, and then the specimen was cycled to failure at the second. Strain ratios of 0.5 and 4 were chosen for this test series. At the strain ratio of 0.5, the combination of stresses chosen was that corresponding to specimen 5133, for which the crack size versus cycle fraction data are given in Fig. 2. The mean life observed for this combination of stresses was 2.08×10^5 cycles. At the strain ratio of 4, the combination of stresses chosen was that corresponding to specimen 5129. The mean observed life for this case was 1.93×10^5 cycles. The applied stresses to the specimens therefore

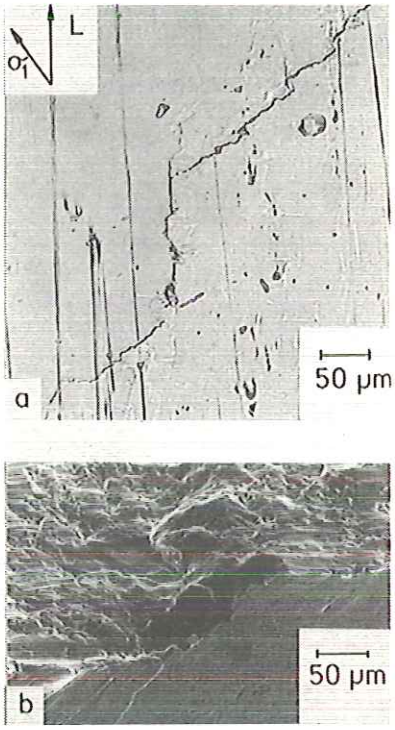

Fig 4 Fractographs: (a) initial growth along the longitudinal direction in specimen 5129 ($\lambda = 4$, N_f = 128 000 cycles). This is followed by growth normal to the maximum principal stress. The longitudinal axis is marked L, and the direction of the principal axes is indicated; (b) scanning electron micrograph of the region of early shear growth in specimen 5129

resulted in equivalent lives for the two strain states. To simplify expression of the results, a mean life of 1.99×10^5 cycles was obtained by averaging over all the observed lives for the two strain ratios, and the results of the varying strain ratio tests are expressed relative to this average. The results of this test series are given in Table 1. It can be seen that the initial cycles at a strain ratio of 0.5 have little effect on the overall life, since the observed total life fractions are grouped around 1. Initial cycles at the strain ratio of 4 do result in some reduction in the total life, since the mean life fraction is now 0.72, and no value was greater than 0.9.

The micromechanisms were therefore investigated for tests at an initial strain ratio of 4. A cycle fraction of 0.18 was first imposed at a strain ratio of 4, and the specimen was cycled to failure at a value of 0.5. Data on the development of cracking are given in Fig. 5. The initial cycles at the strain ratio of 4 resulted in the rapid initiation of a 110 μm long longitudinal shear crack from an inclusion. However, when the strain ratio was changed to 0.5, this crack did not propagate further to any greater extent. Instead, a crack propagated directly from the

Table 1 Results of tests in which the strain ratio was varied

Initial strain ratio	*Second strain ratio*	*Initial cycle ratio applied*	*Total cycle ratio at failure*
0.5	4	0.17	0.63
0.5	4	0.17	0.97
0.5	4	0.39	1.04
0.5	4	0.49	1.4
4	0.5	0.13	0.86
4	0.5	0.18	0.85
4	0.5	0.18	0.68
4	0.5	0.4	0.54
4	0.5	0.4	0.69
4	0.5	0.5	0.75
4	0.5	0.5	0.7

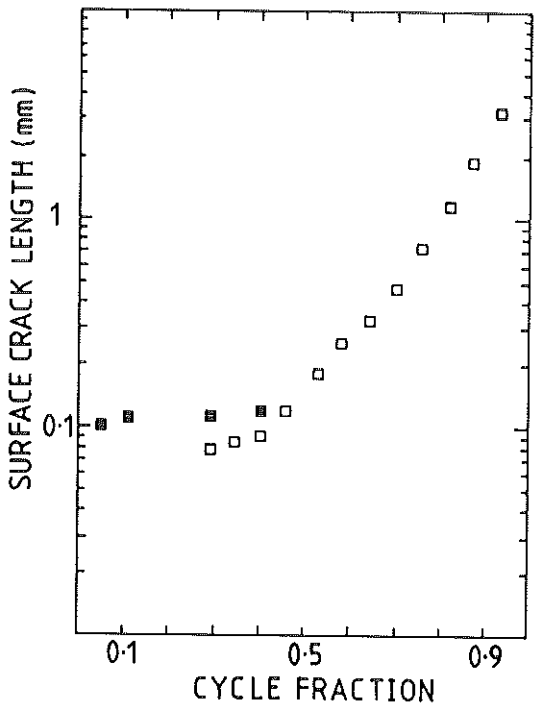

Fig 5 Surface crack length versus cycle fraction for specimen 5136, with 35 000 cycles at $\lambda = 4$ followed by cycling to failure at $\lambda = 0.5$. The number of cycles to failure was 169 600. The initial shear growth is denoted by the closed squares, while the tip-to-tip length of the dominant crack that led to failure is given by the open squares

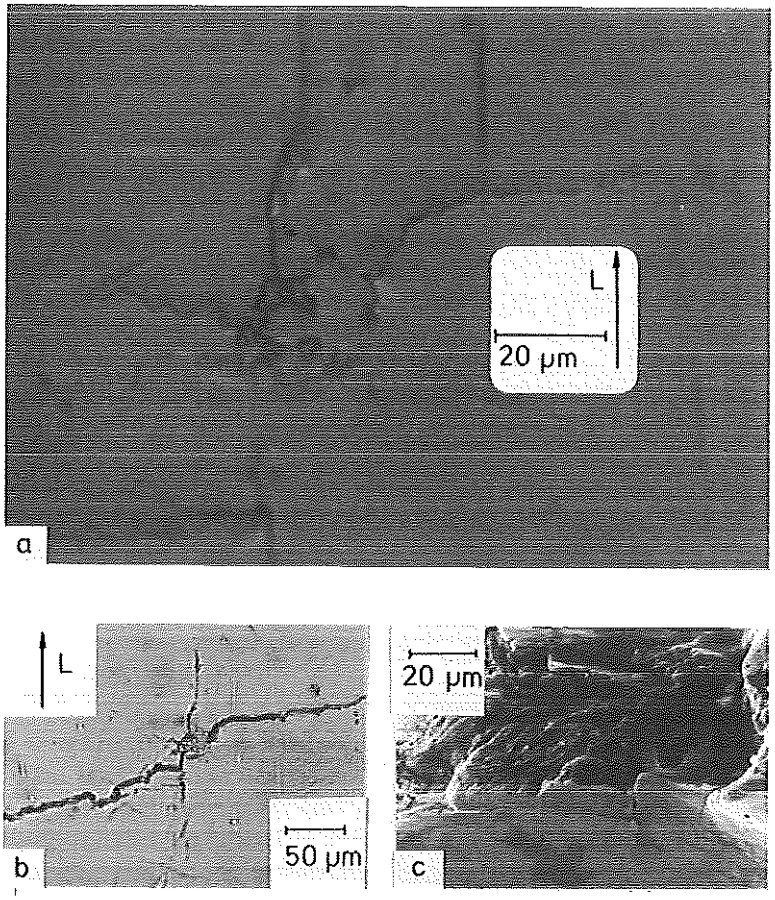

Fig 6 Fractographs: (a) replica taken on specimen 5136 at 70 000 cycles. The inclusion that initiated failure may be seen in the middle of the figure. The initial shear crack extends from the top and bottom of the inclusion. The crack that led to failure is growing away from the inclusion to the right. (b) Replica taken on specimen 5136 at 160 000 cycles, just prior to failure. The dominant Mode I crack may be compared with the shear crack, which has not grown appreciably. (c) Scanning electron micrograph of the initiation site of specimen 5136, showing the initiating inclusion, the initial shear crack, and the fracture surface of the dominant crack

inclusion which had initiated the shear crack, Fig. 6. This crack, which was perpendicular to the maximum principal stress direction corresponding to a strain ratio of 0.5, led to separation of the specimen.

Discussion

Micromechanisms

The simple form of the Kandil *et al.* parameter has been found to provide an adequate correlation for the uniaxial, torsional, and tension plus torsion tests,

although the latter are confined to in-phase loadings in this study. This is therefore of use in design and fatigue life prediction. Indeed, the data in Fig. 1 implies that employing this parameter, together with the uniaxial fatigue data for the material, gives a good description of the multiaxial fatigue performance. Predictions are within a factor of two on life at short and intermediate lives, and are conservative as the fatigue limit is approached. Data at lives in excess of 10^6 cycles are scarce, but a more comprehensive investigation at long lives on a steel at a similar strength level suggests that the fatigue limit depends on strain state, and that the uniaxial data represents a lower bound (**20**). However, the correlation has been achieved in the face of considerable differences in the micromechanisms of fatigue crack initiation and growth for the varying strain ratios.

Taking the micromechanisms for lives around 10^5 cycles as representative, it has been found that, for strain ratios of 0.5 and 1.5, the development of fatigue cracks resembles that observed in uniaxial fatigue, with the majority of the smooth specimen life (~85–88 per cent) being spent in the propagation of short cracks of less than 1 mm total surface length. The development of the cracks is relatively slow, with 100 μm surface length being reached only at 45–50 per cent of the total life. The mode of propagation is by Stage II, or Mode I.

In contrast, the development of cracks at a strain ratio of 4 resembles the behaviour in pure torsion. The cracks reach a correspondingly greater surface length at each cycle fraction, as shown in Fig. 2. A 100 μm surface length is reached at 18 per cent of the total life, and 1 mm surface length by 70 per cent of life. Thus, the propagation stage becomes more important. These tests also show an extended Stage I portion, with Stage I surface lengths between 115 μm and 200 μm being observed. A Stage I to Stage II transition then occurs. The Stage I propagation is along the direction of the aligned inclusions in the material, rather than on the plane of maximum shear, as predicted from continuum analysis. Strictly, the Stage I growth does not fall within the definition proposed by Forsyth, since it is not crystallographic, and is not at sizes less than a grain size (**21**)(**22**).

These differences in micromechanism imply that fatigue life predictions based on the correlation discussed above may be made only with considerable caution. The material response to the variable amplitude and out-of-phase loadings which are commonly encountered in service appears uncertain. For this material, it is not possible to base the choice of the correlating parameter on a single observed initial micromechanism of growth, occurring for all strain ratios, as has been possible in other materials (**8**).

Interactive effects

The contrasting development of fatigue damage for the different strain ratios, Fig. 2, suggests that interactive effects could potentially occur so as to reduce the total overall life if varying strain ratios are applied to the material. The

results of the tests (Table 1), showed no strong interactive effects. The tests with initial cycles at a strain ratio of 0.5 showed lives grouped around the mean life of the constant strain ratio tests. This is not unexpected, as micromechanistic arguments suggest that only tests with an initial strain ratio of 4 would show an interactive effect, leading to a life reduction, since it is this strain ratio which produced early initiation and longer surface crack lengths at a given cycle ratio.

The strain ratio of 4 is able to initiate 100 μm surface cracks at cycle ratios between 0.1 and 0.2, whereas the presence of a crack of this size corresponds to a cycle ratio of 0.45 at the strain ratio of 0.5. If fatigue damage is equated to surface crack length (**23**), it is apparent that considerable scope therefore exists for an overall reduction in life if initial cycles at a strain ratio of 4 are followed by cycling to failure at the ratio of 0.5. In both strain ratios, the crack that leads to separation of the specimen is a crack propagating by Mode I and a physical mechanism therefore exists whereby the different crack systems can interact.

The tests with an initial strain ratio of 4 did show a tendency to fail at shorter lives (Table 1). However, the effect was not strong, and no value of life in the varying strain ratio tests fell shorter than the observed scatterband in the constant strain ratio tests. The strongest interaction, and greatest reduction in life, would be expected to occur for a relatively small initial life fraction, of between 0.1 and 0.2 as discussed above. However, this condition was no more damaging than any other. The results of the micromechanistic observations (Figs 5 and 6) suggest that this is because the longitudinal shear cracks of length around 100 μm are not effective in instigating accelerated Mode I growth to failure when the strain ratio is changed. The failure crack was found to emanate from the initiating calcium aluminate inclusion, rather than from the tips of the shear crack. This behaviour apparently reflects the differing crack shapes and growth modes in the two cases. Longitudinal shear cracks have been found to adopt a relatively shallow aspect ratio at short crack lengths in this steel under pure torsion. For cracks around 100 μm, it was found that the ratio of the depth to the half surface length was 0.15 (**11**). Similar observations on crack shape have been made for shear cracks growing along aligned inclusions in SAE 1045 steel (**13**).

Equating the observed surface length to the fatigue damage may not give an equivalent description for the two strain states, since the mechanism of growth and the shapes of fatigue cracks are different. Further studies of the development of cracking into the depth, and of the Stage I to II transition, are required. However, it should be noted that even when the damage curves were expressed in terms of crack depth for the SAE 1045, this failed to bring the torsional data into agreement with that for the other strain ratios (**13**).

The fact that the shear crack is not as damaging as would be deduced from its surface length is consistent with the proposal (**6**) that cracks growing along the surface, labelled Case A cracks, are not as dangerous as cracks growing away from the surface (Case B). It has also been pointed out that it is geometrically difficult for a Mode I branch crack to form from a crack growing in Mode III

(24). This may explain why the dominant crack emanated from the debonded inclusion, rather than from the tips of the shear cracks. Clearly, this work needs to be extended to include high and low amplitude sequences, other strain ratios, and ultimately, to non-proportional loading.

Conclusions

(1) Tension plus torsion fatigue tests have been performed on smooth specimens of a quenched and tempered steel, and a correlation of the fatigue data, within a factor of two on life, has been achieved at short and intermediate lives using a parameter based on a critical plane theory of multiaxial fatigue.

(2) The correlation has been achieved despite the differences in the micro-mechanisms of fatigue crack initiation and growth that occur for the varying strain ratios. For lives around 10^5 cycles, the mechanisms for strain ratios of 0.5 and 1.5 are similar to those observed in uniaxial fatigue, with similar crack sizes being reached at similar life fractions. At a strain ratio of 4, relatively early initiation occurs on longitudinal shear planes and the behaviour resembles that under pure torsion.

(3) A transition to Stage II does, however, occur at the strain ratio of 4. Nevertheless, appreciably longer surface crack lengths occur for given life fractions, as compared with the lower strain ratios.

(4) Tests have been performed in which the strain ratio is varied so as to investigate possible interactive effects. Earlier initiation at a strain ratio of 4 does lead to some reduction in the overall life.

Acknowledgements

Thanks are due to D. Howkins for his painstaking assistance with the experimental work, and M. S. Starkey for advice on replica techniques. The paper is published by permission of Dr P. Watson, General Manager, Product Development, GKN PLC.

References

(1) WATSON, P. and HILL, S. J. (1982) Fatigue life assessment of ground vehicle components, *Design of fatigue and fracture resistant structures, ASTM STP 761*, ASTM, Philadelphia, PA, pp. 5–27.

(2) WETZEL, R. M. (Editor) (1977) *Fatigue under complex loading: analysis and experiments*, Society of Automotive Engineers, Warrendale, PA.

(3) MORROW, J.-D. and SOCIE, D. F. (1981) The evolution of fatigue crack initiation life prediction methods, *Materials, experimentation, and design in fatigue* (edited by SHERRATT, F. and STURGEON, J. B.), IPC Science and Technology Press, Guildford, pp. 3–21.

(4) LANDGRAF, R. W. (1979) Control of fatigue resistance through microstructure-ferrous alloys, *Fatigue and microstructure*, ASM, Metal Park, Ohio, pp. 439–466.

(5) BROWN, M. W. and MILLER, K. J. (Editors) (1985) *Multiaxial fatigue, ASTM STP 853*, ASTM, Philadelphia.

(6) BROWN, M. W. and MILLER, K. J. (1973) A theory for fatigue under multiaxial stress–strain conditions, *Proc. Instn mech. Engrs*, **187**, 745–755.
(7) FASH, J. W., SOCIE, D. F., McDOWELL, D. L. (1985) Fatigue life estimates for a simple notched component under biaxial loading, *Multiaxial fatigue, ASTM STP 853*, ASTM, Philadelphia, pp. 497–513.
(8) SOCIE, D. F., WAILL, L. A., and DITTMER, D. F. (1985) Biaxial fatigue of Inconel 718 including mean stress effects, ibid, pp. 463–478.
(9) TIPTON, S. M. and NELSON, D. V. (1985) Fatigue life predictions for a notched shaft in combined bending and torsion, ibid, pp. 514–552.
(10) BROWN, M. W. and MILLER, K. J. (1982) Two decades of progress in the assessment of multiaxial low-cycle fatigue life, *Low cycle fatigue and life prediction, ASTM STP 770*, ASTM, Philadelphia, pp. 482–499.
(11) HURD, N. J. and IRVING, P. E. (1985) Smooth specimen fatigue lives and microcrack growth modes in torsion, *Multiaxial fatigue, ASTM STP 853*, ASTM, Philadelphia, pp. 267–284.
(12) FORSYTH, P. J. E. (1961) A two stage process of fatigue crack growth, *Proc. Crack Propagation Symposium*, pp. 76–94, Cranfield, UK.
(13) HUA, C. T. and SOCIE, D. F. (1984) Fatigue damage in 1045 steel under constant amplitude biaxial loading, *Fatigue Engng Mater. Structures*, **7**, 165–179.
(14) KANDIL, F. A., BROWN, M. W., and MILLER, K. J. (1982) Biaxial low cycle fatigue fracture of 316 stainless steel at elevated temperatures, *Mechanical behaviour and nuclear applications of stainless steel at elevated temperatures*, The Metals Society, London, pp. 203–209.
(15) LOHR, R. D. and ELLISON, E. G. (1980) A simple theory for low cycle multiaxial fatigue, *Fatigue Engng Mater. Structures*, **3**, 1–17.
(16) FROST, N. E., MARSH, K. J., and POOK, L. P. (1974) *Metal fatigue*, Clarendon Press, Oxford.
(17) KUNIO, T., SHIMIZIN, M., YAMADA, K., SAKURA, K., and YAMAMOTO, T. (1981) The early stage of fatigue crack growth in martensitic steel, *Int. J. Fracture*, **17**, 111–119.
(18) FORREST, P. G. (1963), *Fatigue of metals*, Pergamon Press, Oxford.
(19) LANKFORD, J. (1977) Initiation and early growth of fatigue cracks in high strength steel, *Engng Fracture Mech.*, **9**, 617–624.
(20) TANAKA, K., MATSUOKA, S., and KIMURA, M. (1984) Fatigue strength of 7075-T6 aluminium alloy under combined axial loading and torsion, *Fatigue Engng Mater. Structures*, **7**, 195–211.
(21) JACQUELIN, B., HOURLIER, F., and PINEAU, A. (1985) Crack initiation under low-cycle multiaxial fatigue, *Multiaxial fatigue, ASTM STP 853*, ASTM, Philadelphia, pp. 285–313.
(22) BROWN, M. W. and MILLER, K. J. (1979) Initiation and growth of cracks in biaxial fatigue, *Fatigue Engng Mater. Structures*, **1**, 231–246.
(23) IBRAHIM, M. F. E. and MILLER, K. J. (1980) Determination of fatigue crack initiation life, *Fatigue Engng Mater. Structures*, **2**, 351–360.
(24) POOK, L. P. (1980) The significance of Mode I branch cracks for combined mode failure, *Fracture and Fatigue* (Edited by RADON, J. C.), Pergamon Press, Oxford, pp. 143–154.